JOURNAL OF MATERIALS SCIENCE 31 (1996) 5271–5279

Ball milling of barium ferrite in air and vacuum

W. A. KACZMAREK
Institute of Advanced Studies, Research School of Physical Sciences and Engineering, The Australian National University, Canberra, ACT 0200, Australia

The effects of prolonged milling in air and vacuum on $BaFe_{12}O_{19}$ ionic crystal structure and particles morphology have been analysed. X-ray diffraction, scanning electron microscopy and thermal analysis experiments show that for vacuum-milled material the ordered structure transforms progressively into a stable disordered nanocrystalline phase. For air-milled samples, apart from structural transformation, chemical decomposition was found.

1. Introduction

Mechanical treatment of ferrite materials has become extremely important in many processes in the technology of magnetic materials during the last few decades. The overall properties of materials are governed by a complex combination of intrinsic and extrinsic properties. An intrinsic property, such as saturation magnetization, is determined by material composition, whereas an extrinsic property, such as magnetic coercivity, is, to a large extent, determined by the microstructure which is in turn influenced strongly by the processing procedures. Mechanochemical [1] changes induced by intensive grinding of non-metallics in this class of materials include the following: (1) polymorphic transformations and alterations in magnetic properties of the bulk phase; (2) mechanical activation and changes in solid surface properties; (3) recrystallization and amorphization; (4) mechanochemical solid state reactions either at the surface or in the bulk.

While the nature of mechanochemical reactions involving non-metallics has advanced somewhat [2], the fundamental processes governing the evolution of structure, kinetics, and thermodynamics of resulting chemical or physical transformations remain incompletely understood. Their elucidation requires more empirical studies. Recently we have shown that complete phase transformation of haematite (Fe_2O_3) into magnetite (Fe_3O_4) can be accomplished by room-temperature ball milling [3]. For the material, it was found that while milling in air does not promote transformation, with the same milling conditions in vacuum, pure nitrogen or argon, the process is surprisingly fast. The decrease of partial oxygen pressure is the main factor determining process effectiveness. The aim of the present work was to exploit improved understanding of the milling process and the greater versatility of modern high-energy mills to reconsider and expand on earlier work relative to the fine grinding of the complex oxide material ($BaO \cdot 6Fe_2O_3$). In a subsequent paper, we will report and use the results to understand the very surprising phenomena that occur in wet milling of the same material [4].

Barium ferrite is used extensively in the permanent magnetic industry. Other examples of applications of this technically important material are the use of fine powders as pigments (at the nanoscale) in high-density recording media, or compacts (submicrometre powders) for high-frequency devices. Commercial milling techniques are used in magnetic materials technology to reduce the particle size from multidomain to magnetically preferred single-domain dimensions. The effect of ball-milling and annealing on the intrinsic coercivity of barium ferrite powders has been studied for dry-milled (in air) [5] and wet-milled powders [6]. In general, after a relatively short time (20–50 h) of milling of dry or wet conditions, an increase of coercivity was observed. This behaviour can be expected, because the milling process reduces the particle size from multidomain to single domain (≈ 1 μm). However, prolonged milling decreases both coercivity and magnetic saturation. The first explanation of the effect assumes that defects are introduced by milling with the generation of superparamagnetic size fractions, or the existence of a second phase with saturation magnetization and a Curie temperature lower than that of the bulk material [5]. However, recently more attention has been focussed on morphological factors as a determinant of material properties. Such microstructure-related interpretations are based on generation of a nanostructured state, with a fraction of the particle volume taking on a disordered nature [7]. The magnetic implications of this effect include a decrease of magnetic saturation, with an increase in the fraction of small-volume crystal blocks with an effective non-magnetic surface layer (predominantly at the *c*-plane surfaces) [8]. The temperature dependence was ascribed to magnetic ions (ferrimagnetic-type magnetic exchange interaction) at the nanocrystal surface layers. These would have a weaker exchange field than internal magnetic ions separated by dislocation blocks. This behaviour is different from earlier proposed explanations that involve superparamagnetic fine particles, because is known that the fraction of very small volume particles is relatively small, even for the samples milled for hundreds of hours.

0022–2461

In this study we examined ball milling of barium ferrite $BaFe_{12}O_{19}$ in air, and in vacuum. We were particularly interested in particle morphology, structural and chemical stability of the dry milled ferrite powder. The study focused on the way in which the disorder is achieved in this permanently and strongly ordered ionic compound.

2. Experimental procedure

2.1. Material

As starting material, commercially available pure (99.99 wt %) barium dodecairon nonadecoxide $BaFe_{12}O_{19}$ ferrite powder with a particle-size distribution in the 0.5–50 μm range (Alfa Products/Jonson Matthey) was used. Powder examination by X-ray diffraction (XRD) technique shows perfect hexagonal structure with space group P63/*mmc*. This is characteristic of M-type ferrites. Fig. 1 shows scanning electron micrographs. Figs 5 and 6, below, include XRD patterns of the pre-milled powder for comparison with milled material.

2.2. Procedure

Prior to milling, two samples (each 10 g) of the powder were annealed for 1 h at ~700 K to remove adsorbed water molecules. The milling in air and "normal" vacuum (10^2–10^3 Pa) was conducted in a vertical stainless steel mill (Uni-Ball) operating in high energy mode [9]. Four 67 g magnetic steel balls with a chrome-hardened surface, were employed during the process. The effective mass of balls in the external magnetic field was ~600 g and the ball to powder weight ratio was ~60:1. More information concerning the type of energy transfer in the mill is available elsewhere [3]. The gas atmosphere inside the vial was controlled by a pressure valve. In this way, both air under normal pressure, and a vacuum, were employed in the preparations. Samples were taken from the vial at different stages of milling (190, 360, 590, 690 and 1000 h) for morphological and structure analysis. Particle morphology was examined by direct observation of gold-coated samples on a Jeol SEM 6400 scanning electron microscope. The structural characterization was performed using a Philips X-ray powder diffractometer employing CoK_α ($\lambda = 1.789$ nm) radiation (scan rate 2 deg min^{-1}) with CD-ROM JCPDS-database and a PC fitting program for detailed analysis of XRD patterns. The calorimetric and thermogravimetric experiments were performed in a Shimadzu DSC-50 and TGA-50H thermoanalysis system, on ~20 mg material under a dynamic pure argon atmosphere with a flow rate of 50 ml min^{-1}. The temperature sweep rate was 15 deg min^{-1} for DSC and 30 deg min^{-1} for TGA.

3. Results and discussion

3.1. SEM analysis of barium powder milled in air

Scanning electron micrographs of pre-milled material are given in Fig. 1. A broad dispersion of particle size is well visible; however, most are in the range 1–5 μm. The shape of the particles can be best characterized as highly irregular. In Fig. 2, results of SEM analysis performed on different samples from air-milled barium ferrite powder are presented (samples A190–A1000). As can be seen, the particle morphology is very different from that of the starting material. Independently of milling time, all particles have a more spherical shape. The particle size was found to be milling-time-dependent as can be estimated from the micrographs. The final 1000 h milled sample shows the smallest particles, with an average size of 0.3 μm. As the milling progresses, cf. Fig. 2d–h, the powder was found to be more homogeneous as the grinding affects mostly the biggest particles. Particles above 1 μm can be found for powder milled up to 590 h. Longer grinding time causes the powder to become homogeneous in size with a narrowing in distribution, estimated to be in the range 0.1–0.5 μm (A1000). For A190 sample at high magnification (cf. Fig. 2b) the particles exhibit a characteristic "stairs" type of surface morphology (similar to edge dislocations in monocrystals). We assume that this effect is due to "mechanical" anisotropy of the barium ferrite crystal structure which is of layered form. The hexagonal oxygen (barium ions included) layers, which are perpendicular to the hexagonal crystal anisotropy axis,

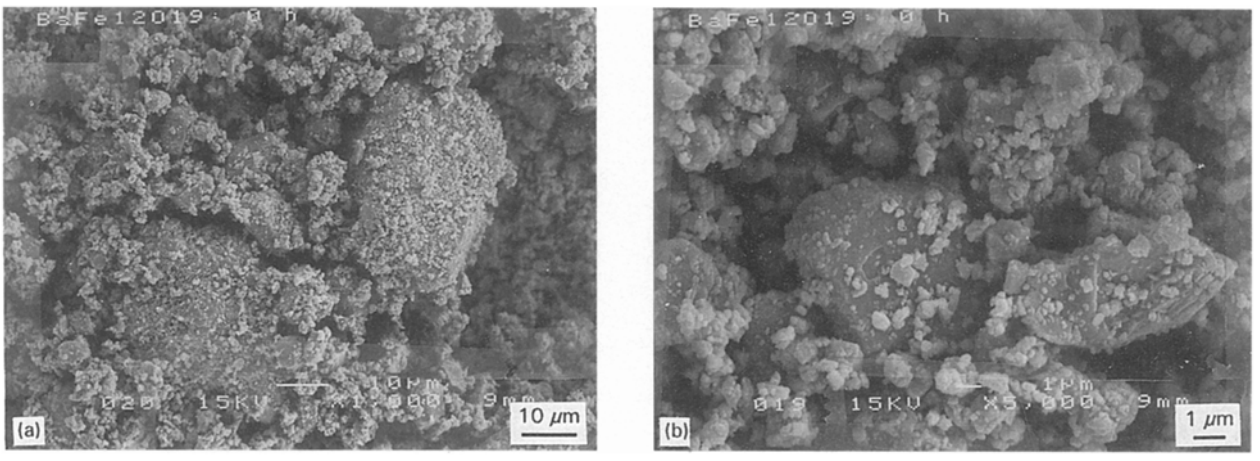

Figure 1 Scanning electron micrographs of pre-milled $BaFe_{12}O_{19}$ powder.

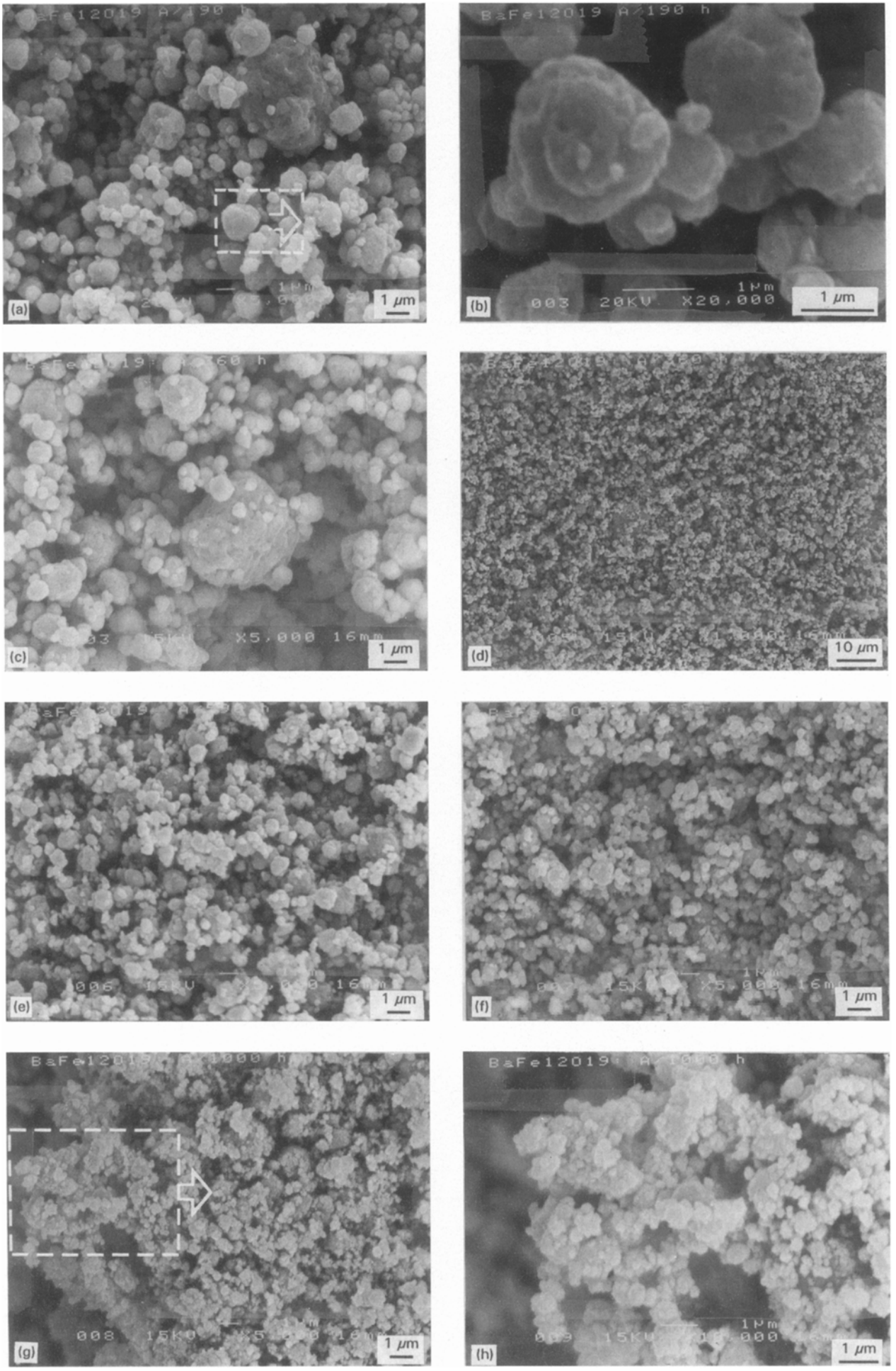

Figure 2 SEM analysis versus milling time performed on air-milled barium ferrite powder. The milling times were (a, b) 190 h, (c, d) 360 h, (e) 590 h, (f) 690 h, (g, h) 1000 h.

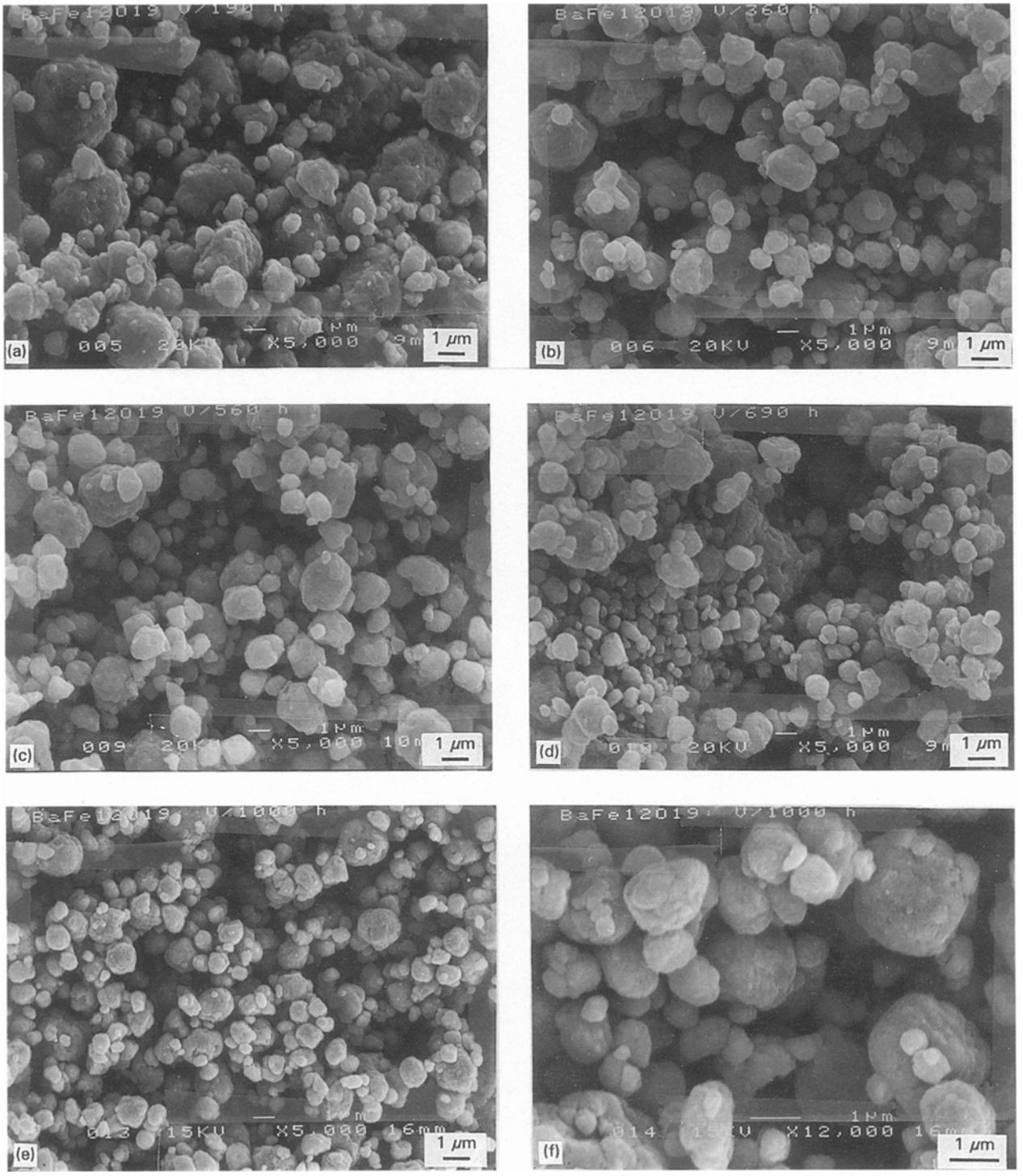

Figure 3 SEM analysis versus milling time performed on vacuum-milled barium ferrite powder.

are convenient as cleavage surfaces, because, as is well known, all preparation techniques yield more or less regular hexagonal platelet particles [10, 11].

3.2. SEM analysis of barium ferrite powder milled in vacuum

In Fig. 3, scanning electron micrographs of barium ferrite milled in vacuum are presented. We found that grinding in a vacuum yield a different particle morphology as compared to samples processed for the same time period in air. Thus, there is not such an apparent particle size decrease with milling time as in air. After the first 590 h the size remains essentially constant. The average particle size is close to 1 μm even after 1000 h. Similar reshaping (to spherical) and initially characteristic "stairs" type of surface can be observed, but for the last sample, V1000 (cf. Fig. 3e–f), different surface morphology is visible. This effect is milling-time-dependent and Fig. 4 shows typical details at higher magnification. In Fig. 4a, the cluster of small ~1 μm particles around a larger one, ~10 μm, is visible. We assume that the effect is due to strong magnetic interactions where the larger particle has a higher magnetic remanence. This will be discussed in detail below. During the course of milling, the small particles and a large one are "alloyed" together, this behaviour is similar to mechanical alloying of metal

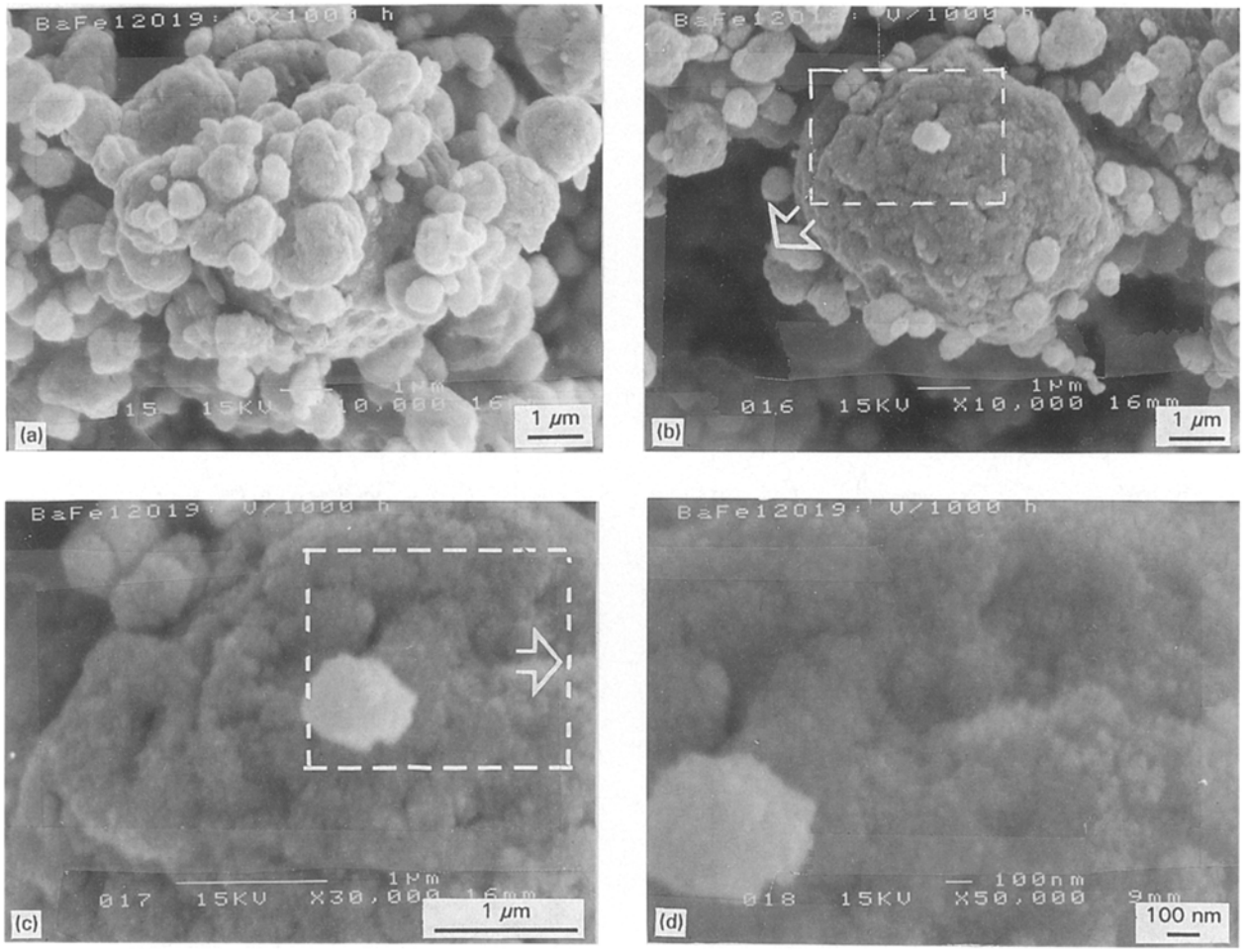

Figure 4 Scanning electron micrographs of V1000 powder particles. Details of (a, b) two characteristic steps in the mechanical "alloying" process and (c, d) particle surface morphology are visible.

particles where simultaneous plastic deformation and fracture of powder particles coexists. In the next stage the particle surface evolves. It was found to be irregular, but the whole particle remains spherical. The surface layer seems to be highly disordered with crystal grains below 50 nm and the amount of these particles increases with milling time. On this point, it is easy to understand why, for barium ferrite powder, the particle size remains above ~ 1 μm. The operating mechanism is more similar to mechanical alloying, than to a simple fracturing process as occurs for the air-milled sample. The nature of this behaviour will be addressed below.

3.3. XRD of barium ferrite powder milled in air

The X-ray diffraction patterns of the materials obtained by milling $BaFe_{12}O_{19}$ powder in air for different periods of time are shown in Fig. 5. As can readily be seen, several distinctive features occur on ball-milling in comparison with the XRD pattern for the pre-milled powder. Firstly, commensurate with the significant peak broadening, the intensities of all of the diffraction peaks decrease with milling time. Indeed for the first pattern, a sample milled for 190 h, the peaks are about twice the widths of the peaks in the starting material. A second development is the broad scattering which extends over the very wide angular range $2\theta \approx 25°–50°$. The extent of this broad peak, centred at $2\theta \approx 37.0° \pm 0.1°$ (190 h); $37.5° \pm 0.1°$ (360 h); $36.8° \pm 0.2°$ (590 h); $38.6° \pm 0.4°$ (690 h) and $38.7° \pm 0.3°$ (1000 h), was further characterized for different milling times using a standard XRD fitting program with a capacity to analyse a maximum of 15 peaks at the same time. The discernible peaks in the $2\theta \approx 25°–80°$ range were fitted individually, allowing the broad feature to be described by a Gaussian curve of full-width at half-height $\Delta(2\theta) = 9.8° \pm 0.2°$ (190 h); $12.1° \pm 0.3°$ (360 h); and $12.4° \pm 0.5°$ (590, 690 and 1000 h). This broad peak is located near the position of the most intense reflection from the (1 0 7) plane of the barium ferrite crystal structure ($2\theta_{1\,0\,7} = 37.51°$). From the analysis of the fits to the XRD data over the scattering region 25°–55° the following values for the fractional area of this broad feature, A_b, as a function of the milling times were found: $A_b \approx 65\%$ (190 h); $\approx 72\%$ (360 h); $\approx 81\%$ (590 h); $\approx 68\%$ (690 h) and $\approx 45\%$ (1000 h). This behaviour, with a maximum in the intensity of the broad peak after 590 h milling, is evident from the overall trend of the XRD patterns shown by Fig. 5. The intensities of all the peaks decrease with milling time (190–360 h), with a tendency for new peaks to occur for longer milling time (690–1000 h). The XRD pattern of the sample milled for 1000 h does allow a semi-quantitative analysis of

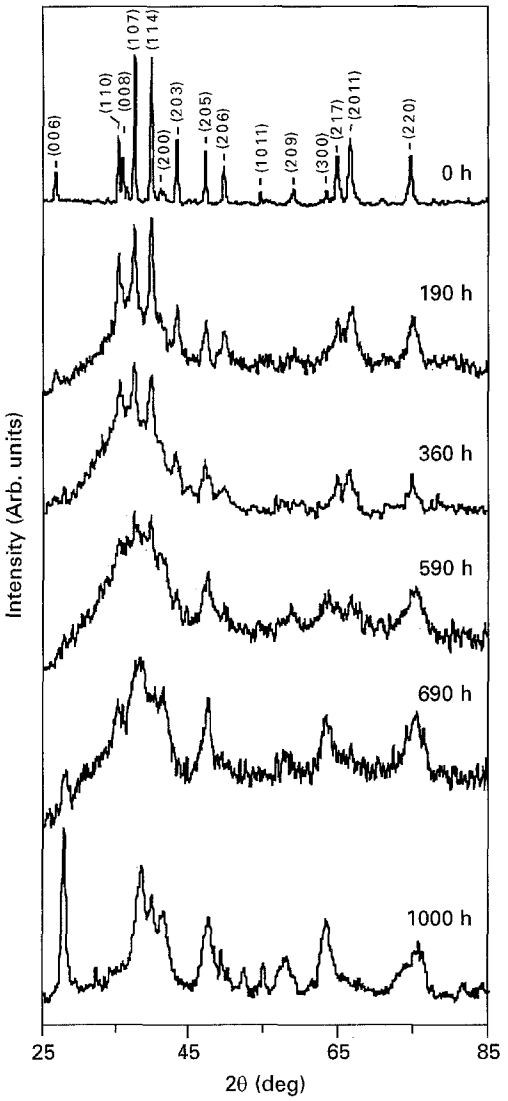

Figure 5 XRD pattern evolution of the $BaFe_{12}O_{19}$ powder milled in air for different periods of time.

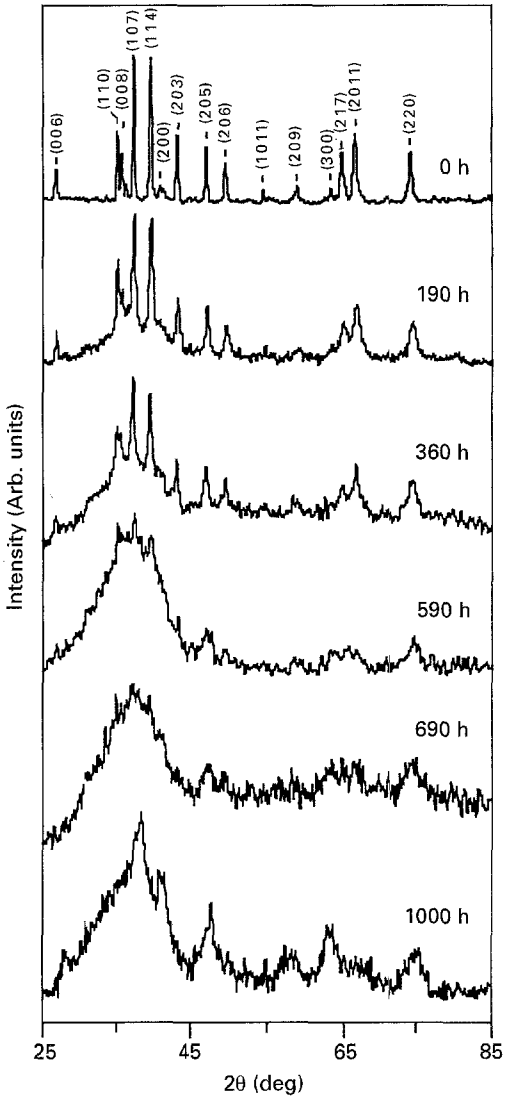

Figure 6 XRD pattern evolution of the $BaFe_{12}O_{19}$ powder milled in vacuum for different periods of time.

the discernible peaks. In particular the (1 0 7) – 37.5°, (1 1 4) – 39.8°, (2 0 5) – 47.16° and (2 0 6) – 49.7° reflections of hexagonal barium ferrite can be indexed along with the following dominant lines of the haematite α-Fe_2O_3 structure (0 1 2) – 28.1°, (1 0 4) – 38.7°, (1 1 0) – 41.6°, (1 1 3) – 47.8°, (0 2 4) – 58.2°, and (1 1 6) – 63.7°. Given the compositional make-up of ferrimagnetic barium ferrite ($BaO \cdot 6Fe_2O_3$), the structure of the paramagnetic α-Fe_2O_3 being stable at room temperature and the resistance of this simple oxide (other than textural effects) to extended dry or wet ball-milling in air [3], this partial decomposition of $BaFe_{12}O_{19}$ to α-Fe_2O_3 on ball-milling in air is not unlikely. Indeed, the most intense barium ferrite XRD reflection $2\theta_{1\,0\,7} = 37.510°$ transforms into the strongest line for haematite $2\theta_{1\,0\,4} = 38.694°$. During continuous mechanical activation, the starting powder undergoes transformations, the most obvious of which are colour changes of the powder. The 1000 h ball-milled sample, A1000, is dark reddish-brown, remarkably different from the dark brown pre-milled $BaFe_{12}O_{19}$ powder. For each milling period, the trend in a colour change is a consequence of structure transformation shown in Fig. 5.

3.4. XRD of borium ferrite powder milled in a vacuum

Fig. 6 shows the XRD pattern evolution for $BaFe_{12}O_{19}$ powder processed in a vacuum. The decrease of the peak intensities and continuous broadening of the Bragg peaks are evidence of the formation of a nanocrystalline phase and the effect is similar to that described above for air-milled powder. The most evident changes here in comparison with Fig. 5 are the absence of strong material decomposition for the 690 h and 1000 h milled powders. However, for the V1000 sample, a weak tendency for the onset of new peaks can be assumed. By employing the same XRD fitting program with a Gaussian shape to data from Fig. 6, it was found that the broad feature is centred and has full-width at half-height: $2\theta = 38.2° \pm 0.7°$ and $\Delta 2\theta = 13.7° \pm 0.4°$ (190 h); $37.5° \pm 0.5°$ and $13.9° \pm 0.4°$ (360 h); $36.8° \pm 0.5°$ and $10.3° \pm 0.3°$ (590 h); $36.6° \pm 0.2°$ and $11.1° \pm 0.4°$ (690 h); $36.4° \pm 0.3°$ and $10.4° \pm 0.5°$ (1000 h), respectively. It is clear from the above that the $2\theta_{1\,0\,7}$ peak is shifted to lower values with increasing milling time. Thus, the $d_{1\,0\,7}$ spacing of the barium ferrite structure increases for vacuum-milled powder, contrary to the trend

observed for air-milled powder. We attribute this effect to mechanically induced structure deformations (responsible for long-range disorder) of vacuum ball-milled material. For air-milled powder the structural decomposition of barium ferrite is due to high oxygen gas adsorption on the particle surface. These effects will be clarified from detailed analysis of thermogravimetric data described below. From an analysis similar to that given above of the fits to the XRD data over the scattering region 25°–55° the following values for the fractional area of broad features, A_b, as a function of the milling times were found: $A_b \approx 65\%$ (190 h); $\approx 76\%$ (360 h); $\approx 78\%$ (590 h); $\approx$ 80% (690 h) and $\approx 79\%$ (1000 h). These values agree well with the behaviour described qualitatively above. We conclude that in powder milled in vacuum the disordering process is continuous. As mentioned above, for the 1000 h milled sample, V1000, a weak tendency for reordering must be taken into consideration. In this way, observed structural changes are different for air- and vacuum-milled powders.

3.5. DSC of barium ferrite powder

For further evaluation, results obtained from DSC for premilled material are presented in Fig. 7. DSC scans were performed in the temperature range 294–1373 K. There is a minimal influence of magnetic history on the DSC curve shape. Both as-supplied and material magnetized preliminarily in a magnetic field of 0.5 T, show characteristic sharp endothermic peaks at $T_c = 727$ K. This temperature is the same as the ferri-paramagnetic transition Curie temperature for barium ferrite. However, the different behaviour observed in a temperature range around 930 K can be related to the existence of weak ferromagnetism in spinel blocks of the barium ferrite crystal structure (observed normally for α-Fe_2O_3 crystals for temperatures up to $T_N = 955$ K).

3.6. DSC and TGA of barium ferrite powder milled in air

Fig. 8 shows DSC curves obtained for barium ferrite milled in air. With progressive milling time the evolution of the DSC scans is apparent. The most characteristic feature of every curve is a broad endothermic peak, the minimum of which shows the Curie temperature related to the processed powder. These observations also suggest, in an indirect way, that the observed dispersion of T_c values is coincident with a particle-size distribution for each powder sample. As was already stated, the lowest particle-size distribution was found for sample A1000. For air-milled barium ferrite there is an interesting dependence of T_c on milling time. The process of partial decomposition of barium ferrite during milling in air is in good agreement with results presented in Fig. 8. It is clear that with increased milling time assumed from XRD results and described above, the magnetic transition temperature, T_c, decreases. In fact, for the last sample (paramagnetic powder at room temperature), the DSC peak minimum is below room temperature, where measurement starts. The minimum observed in Fig. 8 for this sample is due to lack of thermal equilibrium (base line) at the beginning of the scan. Results of magnetic measurements will be presented separately.

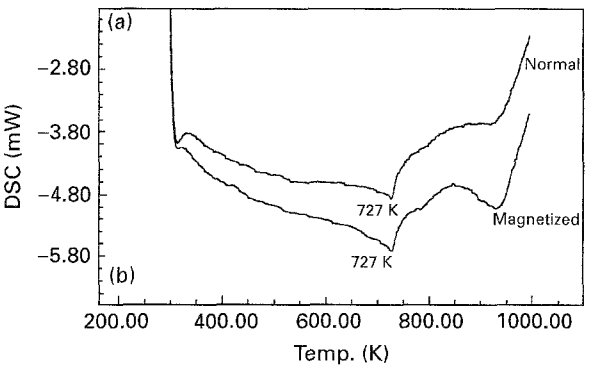

Figure 7 DSC curves of pre-milled $BaFe_{12}O_{19}$ powder, (a) as-supplied and (b) preliminarily magnetized in ~0.5 T magnetic field.

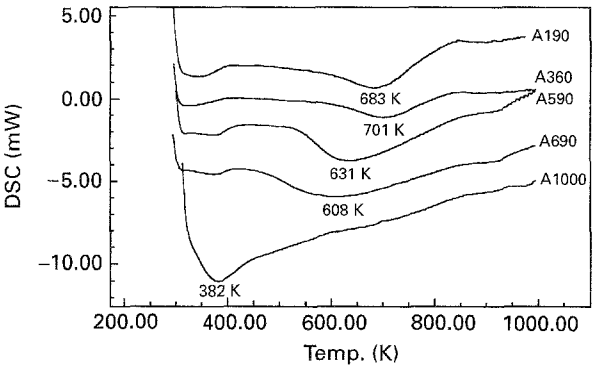

Figure 8 Evolution of DSC curves versus milling time for ferrite powder milled in air. Heat axis units are given as a guide only.

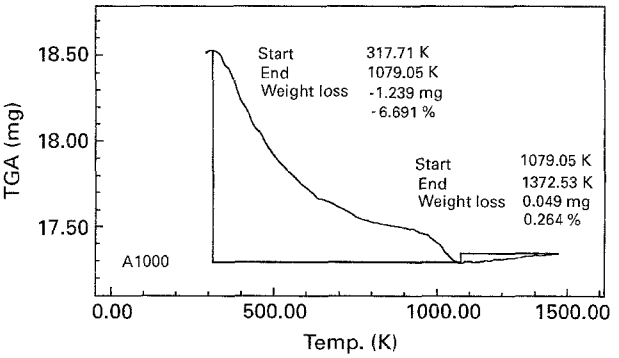

Figure 9 TGA scan for the A1000 sample.

Thermogravimetric analysis (TGA) results of sample A1000 are presented in Fig. 9. The observed weight decrease in the temperature range of 330–1070 K has a significantly high value of 6.62 wt %. As discussed below, this behaviour is characteristic only of air-milled material. We assume that it is mainly oxygen loss that is responsible for the observed behaviour – oxygen gas adsorption on the particle surfaces or dissolution into nanostructured material in the space between nanocrystals inside each powder particle. The number of oxygen molecules, O_2, per one crystallographic barium ferrite unit cell ($2 \times BaFe_{12}O_{19}$) at room temperature, can be obtained by calculation

from the weight loss, and was found to be ~1.2. This result shows that statistically near one additional oxygen atom is connected to one barium ferrite molecule. At the present time it is difficult to discuss this problem in detail, because of the unknown nature of this bonding. It is impossible to distinguish if it is physically or chemically adsorbed. However, we assume that the first is more likely because other gas elements in air can have the same influence as oxygen and a high density of crystal structure defects on the surface can promote physisorption. In the case of chemisorption, it would be difficult to explain further oxidation or decomposition. The final weight decrease in the temperature range 920–1070 K observed in the TGA scan, is attributed to barium ferrite recrystallization. In fact, for this sample, it can be more accurately described as a transformation process between nanostructured (partly decomposed) material and ordered crystalline phase.

3.7. DSC and TGA of barium ferrite powder milled in vacuum

In Fig. 10, DSC scans of barium ferrite powder milled in vacuum are shown. From these results it was found that powders with different milling times show similar reordering kinetics under a continuous heating regime, contrary to air-processed material. In fact, the DSC curve shape is less milling-time-dependent. The minimum of the broad endothermic peak assigned to the Curie temperature, T_c, has a similar value for all powders. However, some changes dependent on the milling time are observed. As the milling proceeds and particle size decreases, the minimum of the endothermic peak at first increases and then decreases. For air-milled samples, the highest temperature where the peak occurs was 701 K (360 h) and for the vacuum sample was found to be 703 K (590 h). Both these temperatures are practically the same, but the milling time is shorter for air-milled powder. The effect is related to particle size. As noted before, a faster particle-size decrease was observed for air-milled powder. The highest value of T_c can be observed for powder with a crystal grain size equal to magnetic single domain size ~0.5 μm (for barium ferrite) [12]. When the particles are larger than 0.5 μm they are multidomain, and when smaller the magnetic parameters decrease because of increasing fine particle specific surface area (magnetic dead layers on the surface) [13]. For sample V1000, a $T_c = 683$ K was found, 10% below the value of bulk barium ferrite. At room temperature, all vacuum-milled powders are magnetic (details of magnetic hysteresis measurements will be published separately).

The TGA scans of powder V1000 (Fig. 11), and A1000 (Fig. 9), are different. The effect observed for vacuum-milled powder has a nearly ten times lower magnitude and has different thermal characteristics. Weight loss can be observed in a narrow range of temperatures: 570–820 K. Subsequently, weight increases over a much broader temperature range, 820–1270 K. We assume that trace gas desorption occurs up to 820 K as the nanocrystal structure is

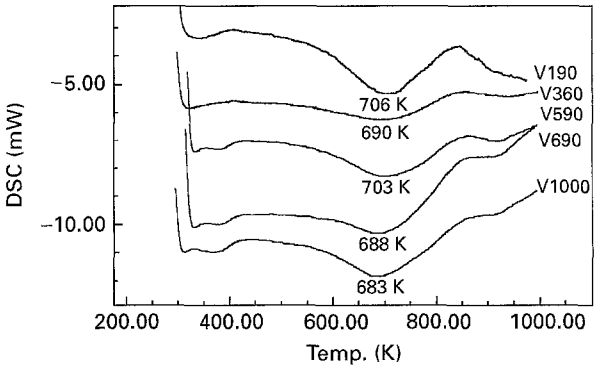

Figure 10 Evolution of DSC curves versus milling time for ferrite powder milled in vacuum. Heat axis units are given as a guide only.

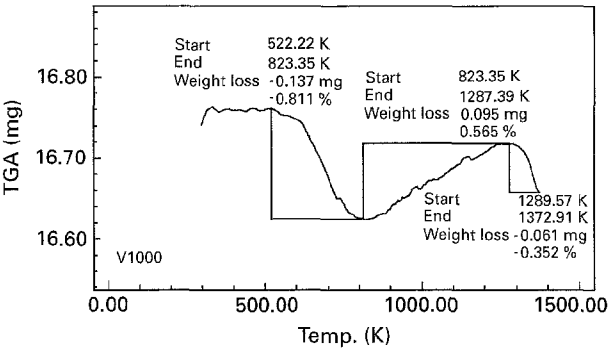

Figure 11 TGA scan for the V1000 sample.

under thermal stress relaxation, and then barium ferrite crystal grain growth requires oxygen (argon used in TGA experiments has oxygen contamination) to fill up its vacancies. The same effect is visible for sample A1000 in the high-temperature range (cf. Fig. 9). During thermal treatment of samples A1000 and V1000, a regrowth of grains of the ordered phase occurs and this process requires further detailed analysis [14].

In summary results from XRD, SEM and thermal analysis experiments emphasise that structural and chemical aspects are directly linked both in the milling process and thermally activated disorder to order transformation.

Acknowledgement

The author thanks Mrs Zhong Li for experimental assistance with the thermal analysis.

References

1. I. J. LIN and S. NADIV, *Mater. Sci. Eng.* **39** (1979) 93.
2. T. KOSMAC and T. H. COURTNEY, *J. Mater. Res.* **6** (1992) 1519.
3. W. A. KACZMAREK and B. W. NINHAM, *IEEE Trans. Magn.* (1994) *IEEE Trans. Magn.*, **MAG-30** (1994) 732.
4. W. A. KACZMAREK and B. W. NINHAM, *Mater. Chem. Phys.* **40** (1995) 21.
5. K. HANEDA and H. KOJIMA, *J. Am. Ceram. Soc.* **57** (1974) 68.
6. W. A. KACZMAREK and B. W. NINHAM, *IEEE Trans. Magn.*, **MAG-30** (1994) 717.

7. H. GLEITER, *Progr. Mater. Sci.* **33** (1989) 223.
8. S. KURISU, T. IDO and H. YOKOYAMA, *IEEE Trans. Magn.*, **MAG-23** (1987) 3137.
9. A. CALKA and A. RADLINSKI, *Mater. Sci. Eng.* **A134** (1991) 1350.
10. R. O. SAVAGE and A. TAUBER, *J. Am. Ceram. Soc.* **47** (1964) 13.
11. W. A. KACZMAREK, B. W. NINHAM and A. CALKA, *J. Appl. Phys.* **70** (1991) 5909.
12. A. H. ESCHENFELDER, "Magnetic bubble technology" (Springer, Berlin, 1981).
13. R. H. VICTORA, *J. Appl. Phys.* **67** (1990) 5161.
14. W. A. KACZMAREK, *J. Mater. Sci.* **31** (1996) 491.

Received 18 January 1994
and accepted 13 February 1996